MOLECULAR
METABOLISM

GDNF family receptor alpha-like (GFRAL) expression is restricted to the caudal brainstem

Cecilia Hes[1,2], Lu Ting Gui[1,3], Alexandre Bay[1], Fernando Alvarez[1], Pierce Katz[1,3], Tanushree Paul[1],
Nadejda Bozadjieva-Kramer[4,5], Randy J. Seeley[4], Ciriaco A. Piccirillo[1,6,7,8], Paul V. Sabatini[1,2,3,*]

ABSTRACT

Objective: Growth differentiation factor 15 (GDF15) acts on the receptor dimer of GDNF family receptor alpha-like (GFRAL) and Rearranged during transfection (RET). While *Gfral*-expressing cells are known to be present in the area postrema and nucleus of the solitary tract (AP/NTS) located in the brainstem, the presence of Gfral-expressing cells in other sites within the central nervous system and peripheral tissues is not been fully addressed. Our objective was to thoroughly investigate whether GFRAL is expressed in peripheral tissues and in brain sites different from the brainstem.

Methods: From *Gfral*:eGFP mice we collected tissue from 12 different tissues, including brain, and used single molecule *in-situ* hybridizations to identify cells within those tissues expressing *Gfral*. We then contrasted the results with human *Gfral*-expression by analyzing publicly available single-cell RNA sequencing data.

Results: In mice we found readably detectable *Gfral* mRNA within the AP/NTS but not within other brain sites. Within peripheral tissues, we failed to detect any *Gfral*-labelled cells in the vast majority of examined tissues and when present, were extremely rare. Single cell sequencing of human tissues confirmed *GFRAL*-expressing cells are detectable in some sites outside the AP/NTS in an extremely sparse manner. Importantly, across the utilized methodologies, smFISH, genetic *Gfral* reporter mice and scRNA-Seq, we failed to detect *Gfral*-labelled cells with all three.

Conclusions: Through highly sensitive and selective technologies we show *Gfral* expression is overwhelmingly restricted to the brainstem and expect that GDF15 and GFRAL-based therapies in development for cancer cachexia will specifically target AP/NTS cells.

1. INTRODUCTION

GDF15 is a critical mediator of the physiologic response to stress [1]. While many cell types are capable of producing and releasing GDF15 [2–4], the circulating GDF15 levels are very low under homeostatic conditions but increase under specific conditions [5]. The physiologic and pathophysiologic states in which GDF15 levels increase are highly varied and include pregnancy [2,6], physical exercise [7], cancer [8], infection [9] and many others [10,11]. Like the broad range of conditions which increase circulating GDF15, the functions of the hormone are equally pleiotropic. Exogenous GDF15 reduces food consumption [12], slows gastric emptying [4], and produces aversive taste responses, nausea and emesis [13]. It has also been shown to modulate the immune system [9] and increase energy expenditure [14,15].

Given the number of tissues and cell types that express and secrete GDF15 and its wide ranging effects on different biological processes, it is somewhat unexpected that the only identified receptor for GDF15, GFRAL (acting as a heterodimer with RET) is expressed exclusively in the brainstem on a small number of cells in the AP/NTS [12,16–18]. However, it is possible that rare *Gfral*-expressing cell populations exist outside the AP/NTS. As *Gfral* is a lowly expressed transcript, even within the AP/NTS [19,20], transcriptomic analysis of *Gfral* in peripheral tissues using qRT-PCR may fail to detect rare *Gfral*-expressing cells [9,12,16,18,20]. Intriguingly, a recent report details GFRAL immunoreactivity broadly across the mouse central nervous system and in multiple peripheral tissues [21], supporting a model of diffuse GDF15 action across multiple GFRAL-expressing cell types and tissues.

Thus, two models of GDF15 have emerged: one in which GDF15 action is restricted to the AP/NTS and another in which GDF15 action is mediated by multiple tissues, we sought to test these utilizing single molecule *in-situ* hybridizations (smISH), two genetic mouse models to

[1]Research Institute of the McGill University Health Centre, McGill University Health Centre, 1001 boulevard de Decarie, Montreal, QC, H4A 3J1, Canada [2]Division of Experimental Medicine, Department of Medicine, McGill University, 1001 boulevard de Decarie, Montreal, QC, H4A 3J1, Canada [3]Integrated Program in Neuroscience, Department of Medicine, McGill University, Room 302 Irving Ludmer Building, 1033 Pine Ave. W. Montreal, QC, H3A 1A1, Canada [4]Department of Surgery, University of Michigan, 2800 Plymouth Rd, Ann Arbor, MI, 48109, USA [5]Veterans Affairs Ann Arbor Healthcare System, Research Service, 2215 Fuller Rd, Ann Arbor, MI, 48105, USA [6]Department of Microbiology and Immunology, Department of Medicine, McGill University, 3775 University Street, Montreal, QC, H3A 2B4, Canada [7]Centre of Excellence in Translational Immunology (CETI), Research Institute of the McGill University Health Centre, 1001 boulevard de Decarie, Montreal, QC, H4A 3J1, Canada [8]Program in Infectious Diseases and Immunology in Global Health, Research Institute of the McGill University Health Centre, 1001 boulevard de Decarie, Montreal, QC, H4A 3J1, Canada

*Corresponding author. Research Institute of the McGill University Health Centre, McGill University Health Centre, 1001 boulevard de Decarie, Montreal, QC, H4A 3J1, Canada. E-mail: paul.sabatini@mcgill.ca (P.V. Sabatini).

Received September 20, 2024 • Revision received November 12, 2024 • Accepted November 18, 2024 • Available online 26 November 2024

https://doi.org/10.1016/j.molmet.2024.102070

Abbreviations

3v	third ventricle	iWAT	inguinal white adipose tissue
AP	area postrema	L.N.	lymph node
ARC	arcuate nucleus	ns	non-significant
CA1	cornu Ammonis region 1	NTS	nucleus of the solitary tract
diH$_2$O	distilled water	OPC	oligodendrocyte precursor cell
DVC	dorsal vagal complex	PC	principal component
EDTA	ethylenediaminetetraacetic acid	PBS	phosphate-buffered saline
FACS	fluorescence-activated cell sorting	qRT-PCR	quantitative reverse transcription polymerase chain reaction
GABA	gamma-aminobutyric acid	RET	Rearranged during transfection
GDF15	growth differentiation factor 15	RI-MUHC	Research Institute of McGill University Health Centre
GFP	green-fluorescent protein	scRNA-seq	single-cell RNA sequencing
GFRAL	GDNF family receptor alpha-like	SEM	standard error of the mean
GW	gestational week	smISH	single molecule *in-situ* hybridizations
IHC	immunohistochemistry	UMAP	uniform manifold approximation and projection
IR	immunoreactivity	UMI	unique molecular identifiers
ISH	*in-situ* hybridizations	v	version
		W	week
		WT	wild-type

---

label *Gfral*-expressing cells [19] and single-cell RNA sequencing (scRNA-seq) data [22—28].

2. MATERIALS & METHODS

2.1. Animals

Mice were bred in the Unit for Laboratory Animal Medicine at the University of Michigan and the Research Institute of McGill University Health Centre (RI-MUHC). Procedures performed were approved by the University of Michigan Committee on the Use and Care of Animals, in accordance with Association for the Assessment and Approval of Laboratory Animal Care and National Institutes of Health guidelines. Alternatively, procedures were approved by the animal care committee of McGill University. We provided mice with *ad libitum* access to food (Purina Lab Diet 5001) and water in temperature-controlled (22 °C) rooms on a 12-hour light—dark cycle with daily health status checks. *Rosa26$^{LSL-eGFP-L10a}$* mice [29], *Gfral^{Cre}* and *Gfral^{CreERT}* mice have been described previously [19]. We used both male and female mice for all studies. *Rosa26^{Sun1sfGFP}* (JAX stock # 030952) mice with germline deletion of the STOP cassette were used as positive controls for green-fluorescent protein (GFP) staining.

2.2. Tamoxifen administration

We dissolved tamoxifen (Sigma) in corn oil and administered to mice via intraperitoneal injection once a day for 5 consecutive days at a concentration of 150 mg/kg. Controls received corn oil-alone. We randomized *Gfral^{CreERT};Rosa26$^{LSL-eGFP-L10a}$* mice and injected tamoxifen or a control injection. All animals were 12 weeks of age at the time of injection and tissue was collected from animals 4 weeks post-injection.

2.3. Tissue collection, embedding and GFP staining

We euthanized *Gfral^{Cre};Rosa26$^{LSL-eGFP-L10a}$* mice and wild-type (WT) controls (*Gfral^{WT}; Rosa26$^{LSL-eGFP-L10a}$*) using isoflurane anaesthesia followed by CO$_2$ asphyxiation. For fixed tissue collection, we perfused mice transcardially perfused with phosphate buffered saline for 3 min followed by 5 min perfusion with 10% formalin. We then collected peripheral tissues and postfixed them for 24 h in 10% formalin before transferring them to 70% ethanol. The tissue was then dehydrated, and paraffin embedded in paraffin by the University of Michigan *in vivo* animal core. We collected, deparaffinized and rehydrated 5 μm-thick paraffin sections. We performed immunohistochemical detection of GFP with the Discovery Ultra instrument from Roche. After antigen retrieval treatment (ethylenediaminetetraacetic acid (EDTA) buffer, 32 min), we incubated sections 24 min at 37 °C with anti-GFP (1:300, #598, MBL) followed by secondary antibody incubation with OmniMap anti-Rb HRP (760—4311, Roche) at room temperature for 20 min, followed by the detection Kit ChromoMap DAB kit (760—4304, Roche). Then, we counterstained the slides with the hematoxylin, and dehydrated, cleared and cover slipped them. For brain tissues, we fixed mice as described above and post-fixed brains in formalin for 24 h prior to transferring them to 30% sucrose for a minimum of 24 h. Subsequently, we sectioned brains as 30 μm free floating sections and then blocked for 1 h in phosphate-buffered saline with 0.1% Triton X-100 and 3% normal donkey serum (Fisher Scientific). We incubated the sections overnight at room temperature in chicken anti-GFP (GFP-1020, Aves). The following day, we washed sections and incubated them with FITC-conjugated secondary antibody (Invitrogen, Thermo Fisher, 1:300). After washing the tissues three times in phosphate-buffered saline (PBS), we mounted them onto glass slides and cover slipped them after covering in mounting media (Fluoromount-G, Southern Biotechnology). For quantification, total nuclei were quantified using Cell profiler [30] and GFP immunohistochemistry was manually counted by a blinded observer.

2.4. Fluorescence-activated cell sorting (FACS) for GFP+ cells

For tissue collection for FACS, we euthanized *Gfral^{Cre};Rosa26$^{LSL-eGFP-L10a}$* mice with isoflurane followed by CO$_2$ and put collected tissues in PBS. The spleen and inguinal lymph nodes were harvested separately from each mouse immediately post-mortem and kept in ∼4 mL of complete RPMI 1640 (Wisent) supplemented with 10% Fetal Bovine Serum, 1% penicillin/streptomycin, 1% HEPES (Wisent), 1% sodium pyruvate (Wisent), 1% Minimum Essential Medium non-essential amino acids (Wisent), gentamycin (50 mg/mL, 100 μL for 500 mL), and 2-mercaptoethanol. Following perfusion with complete RPMI, we mechanically dissociated the spleens and inguinal lymph nodes by gentle disruption using the plunger end of a syringe on a sterile 70 μm cell strainer placed over a Petri dish. We washed cells through the strainer with 10 mL of complete RPMI medium and collected them into 15 mL conical tubes. We then centrifuged the resulting suspension at 400×g for 5 min at 4 °C to pellet the cells. We discarded the supernatant and resuspended the cell pellet in 1 mL of Ammonium-

Chloride-Potassium (ACK) lysis buffer (Thermofisher) and incubated for 30 s at room temperature to lyse erythrocytes. Lysis was terminated by quenching the suspension with 10 mL of complete RPMI medium, followed by another centrifugation at $400 \times g$ for 5 min at 4 °C. We again discarded the supernatant and resuspended the cells in 1 mL of complete RPMI medium. To ensure a single-cell suspension, we passed them through a new 70 μm cell strainer. After a final centrifugation at $400 \times g$ for 5 min at 4 °C, we resuspended the cell pellet in 1 mL of PBS. Cells were counted using a hemocytometer, and the concentration was adjusted to 1×10^6 cells/mL for subsequent staining and analysis.

Cells were then incubated with Fixable Viability eFluor 780 Dye (1:1000, ThermoFisher Scientific, Cat. 65-0865-14) and Fc receptor block (1:50, 2.4G2, BD Biosciences, Cat. 553142) at 4 °C for 15 min. We prepared an antibody cocktail for surface proteins in PBS and added this cocktail to the cells. We then incubated the cells at 4 °C for 20 min before washing them with PBS and fixing them using the eBioscience Foxp3/Transcription Factor Staining Buffer Set (eBioscience). Afterwards, we washed the cells with 1X permeabilization buffer (eBioscience) and incubated them for 45 min at 4 °C with antibody cocktails for detection of cytoplasmic and nuclear proteins. One final wash in PBS was performed before acquiring the cells on the BD LSRFortessa X-20.

We performed extracellular staining using the following antibodies (dilution, clone, company, catalog number): anti-mouse CD45.2 BUV395 (1:100, 104, BD Biosciences, Cat. 564616), anti-mouse CD3 BUV737 (1:100, 17A2, BD Biosciences, Cat. 612803), anti-mouse CD4 Alexa Fluor 700 (1:100, RM4-5, Biolegend, Cat. 100536), anti-mouse CD8α-PerCP-Cy5.5 (1:100, 53—6.7, BD Biosciences, Cat. 551162), anti-mouse CD11b V450 (1:100, M1/70, Invitrogen, Cat. 48-0112-80), anti-mouse CD19 PE (1:100, 1D3, BD Biosciences, Cat. 557399). We stained intracellular proteins using the following antibodies: anti-mouse CD3 BUV737 (1:100, 17A2, BD Biosciences, Cat. 612803) and anti-mouse CD4 Alexa Fluor 700 (1:100, RM4-5, Biolegend, Cat. 100536). We used FlowJo v10.10 software (FlowJo, LLC) to analyze data.

2.5. *In-situ* hybridizations (ISH)

Wild-type C57BL/6J mice (Jackson Laboratories) were euthanized and perfused with formalin as described above. We embedded kidney, pancreas, intestine, liver and ovary from each mouse in paraffin and sectioned them at 5 μm thickness and fixed them on slides. We stored these slides at room temperature and then followed the ACD 323100 user manual for the RNAscope® Multiplex Fluorescent Reagent Kit v2 Assay for formalin-fixed paraffin-embedded samples. Briefly, we baked slides in a dry oven at 60 °C for 1 h after which we performed deparaffinization by incubating slides with CitriSolv (Decon Labs Inc.) twice for 5 min, and then with 100% ethanol twice for 2 min. We added H_2O_2 to slides and incubated them for 10 min while protecting them from light. In a steamer with lid, we submerged the slides in 200 mL of hot diH2O for 10 s and then in 200 mL RNAscope® 1X Target Retrieval Reagent for 15 min. After briefly transferring slides to room temperature diH2O, we submerged them in 100% ethanol for 3 min and let them dry. We then applied ∼1—2 drops of RNAscope® Protease Plus to each section and incubated them at 40 °C for 30 min using a HybEZTM oven with distilled water (diH2O) wet paper in the tray.

In addition, we sectioned brain 30 μm thick and fixed these on glass slides which were stored at −20 °C for <36 h. We then followed the ACD 323100 user manual for the RNAscope® Multiplex Fluorescent Reagent Kit v2 Assay for fixed frozen tissue samples in these sections. In this pipeline, we rinsed slides with 1X PBS and incubated them with

H_2O_2 at room temperature for 10 min while protecting them from light. We removed the H_2O_2 and rinsed them with diH2O twice. In a steamer with lid, we submerged the slides in 200 mL of hot diH2O for 10 s and then in 200 mL RNAscope® 1X Target Retrieval Reagent for 5 min. After briefly transferring slides to RT diH2O, we submerged them in 100% ethanol for 3 min and let them dry. We then applied ∼1—2 drops of RNAscope® Protease III to each section and incubated them at 40 °C for 30 min using a HybEZTM oven with diH2O wet paper in the tray.

For both brain and peripheral tissue, after rinsing the slides with diH2O, we hybridized the probes at 40 °C for 2 h. From this point on, we incubated samples at 40 °C in the HybEZTM oven with humid tray and rinsed them with RNAscope® 1X Wash Buffer after each step. We followed the assay applying RNAscope® reagents AMP1, AMP2, AMP3 after which we intercalated HRP channel (15 min), fluorophore (30 min) and HRP blocker (15 min) for each channel in the probes mix. We used a mix of probes containing RNAscope® Mm-*Gfral* (439141-C1) and Mm-*Ppib*-C3 (312281-C3) diluted in probe diluent as specified in the manual user. The fluorophores used were Cy3 (1:1500) for *Gfral* and Cy5 (1:1000) for *Ppib,* diluted in RNAscope® TSA buffer. We applied DAPI dye (1:1000) at the end of the assay and stored samples covered from light for 48—72 h at −4 °C before imaging. Kidney, pancreas, intestine, liver and ovary were imaged on an Olympus BX61, and images of brain sections were taken on a Zeiss LSM780-NLO laser scanning confocal with IR-OPO lasers microscope at the Molecular Imaging Platform at the RI-MUHC, Montreal, CA.

### 2.6. Single-cell RNA sequencing data analysis

We used labeled human single-cell RNAseq databases [22—28] incorporated in scRNAseq v2.16.0 packages in R using SingleR v2.4.1 [31]. Such databases included intestine [26]; endometrium [27]; yolk sac, liver and spleen immune-resident cells [25,28]; pancreas [23], and brain (i.e. cortex and hippocampus) [22,24]. We used uniform manifold approximation and projection (UMAP) coordinates to visualize scaled log-normalized counts of *Gfral*. Databases were processed through Seurat v5, with libraries scaled to 10000 unique molecular identifiers (UMIs) per cell and log-normalized. We identified the most variable genes computing a bin Z-score for dispersion based on 20 bins average expression and regressed UMI counts. We then used principal component (PC) analysis for dimensionality reduction on to the top 2000 most variable genes. First, we used the first 30 PCs for UMAP projections and after integration of multiple samples contained on each database was done with Harmony [32], we used those embeddings for final UMAP projections.

3. RESULTS

We followed a pipeline to interrogate several tissues for *Gfral* expression (Figure 1A). To determine if peripheral tissues expressed *Gfral* mRNA, we first performed ISH for *Gfral* on brain tissue. As a control we also probed for *Ppib* [33]. In align with previous reports [12,17,20], *Gfral* mRNA was readably detectable within the AP/NTS, but we failed to detect it within the hippocampus or acuate nucleus of the mediobasal hypothalamus (Figure 1B). As GFRAL-immunoreactive cells were recently described in peripheral tissues including the kidney, intestine, and liver, we also performed ISH on these tissues [21]. While *Ppib* was detected in all tissues, we failed to observe *Gfral*-expressing cells (Figure 1C).

To complement our ISH approach to detect *Gfral*-expressing cells across a greater number of tissues, we next utilized two genetic mouse models to label *Gfral*-expressing cells with GFP. First, we crossed the
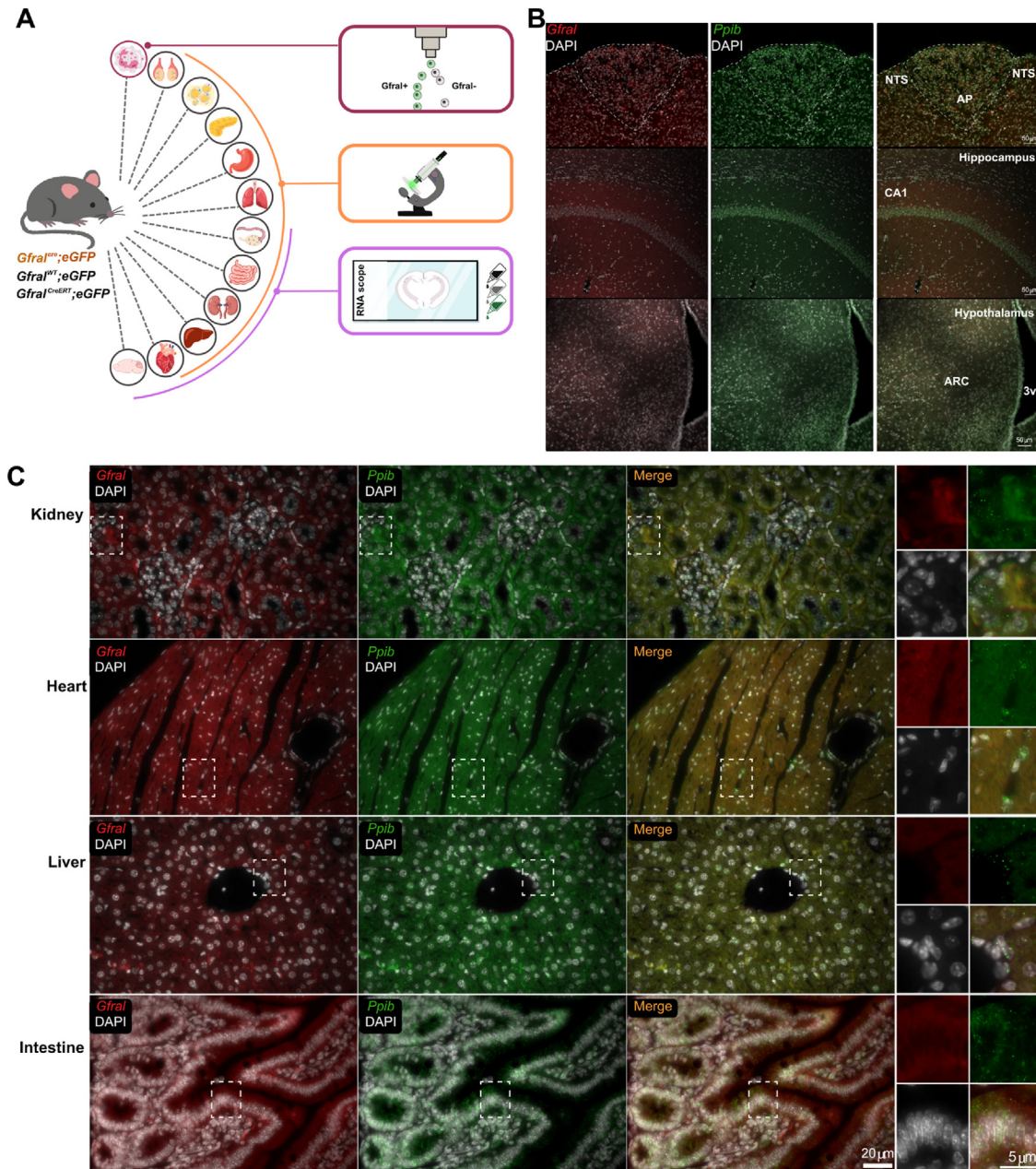
Figure 1: smISH for *Gfral* mRNA in the brain and peripheral tissues. (A) Schematic of the tissue analysis pipeline carried out in mice. We interrogated immune cells, testes, white adipose tissue, pancreas, stomach, lung, ovary, small intestine, kidney, liver, heart and brain and performed either mslSH, FACS-based analysis or RNA scope *in-situ* hybridization. (B) Representative images of smISH for *Gfral* (Red, left panel) and *Ppib* mRNA (Green, center panel) and a merged image (right panel) of mouse area postrema and nucleus of the solitary tract (AP/NTS), hippocampus and medial basal hypothalamus. (C) Representative images of smISH for *Gfral* (Red) and *Ppib* mRNA (Green) with a merged image and higher magnification image of region in boxed (far right panels) of mouse kidney, heart, liver and intestine. DAPI (white) was used to stain nuclei in all images. Dashed lines in A represent the boundaries of the area postrema.

Abbreviations: eGFP = enhanced green fluorescent protein; WT = wild-type; mslSH = single molecule *in-situ* hybridization; FACS=Fluorescence activated cell sorting; AP = area postrema; NTS = nucleus of the solitary tract; ARC = arcuate nucleus; 3v = third ventricle; CA1 = cornu Ammonis region 1.

*Gfral^Cre^* and Cre-dependent *eGFP-L10a* mice, generating *Gfral^Cre^:eGFP* mice, and examined tissues for GFP expression via immunohisto-chemistry (IHC) in adult *Gfral^Cre^::eGFP* mice. As the constitutively active *Gfral^Cre^* allele labels *Gfral*-expressing cells with eGFP regardless of whether *Gfral* was expressed during development or in the fully developed adult mouse, we also adopted a strategy to label *Gfral*-expressing cells exclusively in the fully developed adult mouse. This was accomplished by crossing the tamoxifen-inducible *Gfral*-cre

(*Gfral^CreERT^*) with the Cre-dependent *eGFP-L10a* alleles, generating *Gfral^CreERT^::eGFP* mice. By administering tamoxifen to adult mice, we could ensure eGFP immunoreactivity (IR) was due to active *Gfral* expression in developed tissues.

As expected, both *Gfral^Cre^::eGFP* and *Gfral^CreERT^::eGFP* mice displayed GFP immunoreactivity within the AP/NTS of both models, with the CreERT model displaying reduced number of GFP+ cells (Figure 2). Importantly, in the absence of Cre alleles, we failed to observe GFP
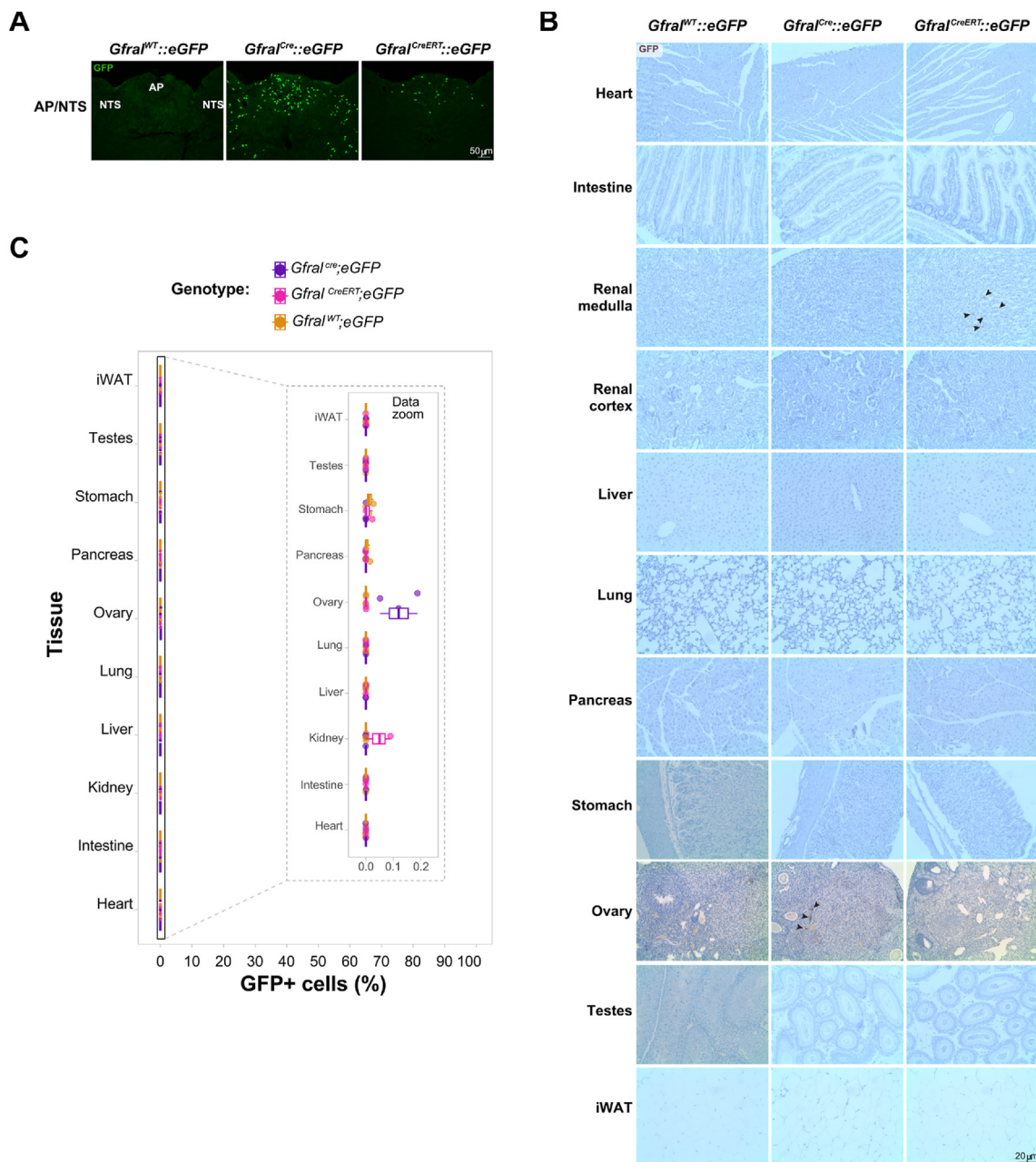
Figure 2: *Gfral* reporter expression in brainstem and peripheral tissues. (A) Representative images of GFP immunoreactivity within the AP/NTS of eGFP-L10a reporter mice lacking Cre recombinase (*Gfral^WT^::eGFP*, left panel), constitutively active *GfralCre::eGFP* (middle panel) and tamoxifen inducible *Gfral^CreERT^::eGFP* mice (right panel). (B) Representative images of GFP immunoreactivity assessed through immunohistochemistry for GFP-labelled cells in mouse tissues from *Gfral^WT^::eGFP* (left panels), *GfralCre::eGFP* (center panels), *Gfral^CreERT^::eGFP* (right panels) animals. (C) Combined boxplot and dotplot of the quantification of GFP positive cells in AP/NTS and peripheral tissues. Three samples per tissue per genotype were quantified. The percentage of cells are given regarding total nuclei on each sample.

Abbreviations: eGFP = enhanced green fluorescent protein; GFP = enhanced green fluorescent protein; AP = area postrema; NTS = nucleus of the solitary tract; iWAT = inguinal white adipose tissue; WT = wild-type.

expression in the *eGFP-L10* reporter (Figure 2A). We then examined multiple tissues from the *Gfral^CreERT^::eGFP* mice including heart, lung, stomach, intestine, liver, pancreas, inguinal white adipose tissue, kidney, testes and ovary (Figure 2B—C). From this analysis, we failed to detect any GFP-labelled cells in most of tissues of *Gfral^CreERT^::eGFP* mice. The exception being kidney where rare cells were detected in the renal medulla where GFP-labelled cells constitute approximately 1 of every 2000 cells (Figure 2B—C). To determine whether we could detect

Gfral-labelled cells in the adult mouse that may have been labelled during embryonic or neonatal development, we also assayed tissues from the constitutively active *Gfral^Cre^::eGFP* mouse. Like what we observed In the *Gfral^CreERT^::eGFP* mouse, we did not detect widespread GFP-IR, rather, the only tissues we detected GFP signal was the ovary (Figure 2B—C). As we failed to detect *Gfral* mRNA by ISH in mouse ovary (Supplemental Fig. 1), we assume this GFP-IR is due to developmental *Gfral* expression and indelible labelling in the adult.

Importantly, a positive control for eGFP staining showed robust GFP-IR, suggesting the failure to detect GFP+ cells in the *Gfral* models was not technical in nature (Supplemental Fig. 2). As GFP-IR was not found within the kidney of Gfral^Cre^:eGFP mice, which should be more sensitive compared with the *Gfral*^CreERT^ model, we expect the GFP-IR detected in Gfral^CreERT^:eGFP mice is due to unspecific recombination or immunoreactivity in the kidney.

As GDF15 has roles regulating the function of numerous immune cell types [34,35], we evaluated GFP expression in various immune cell types from secondary lymphoid tissues (spleen and L.N.s) from *Gfral*^Cre^*::eGFP* mice (Figure 3). Our results show that the frequency or level (Figure 3B—C) of GFP expression in total hematopoietic (CD45+), T (CD3+), B (CD19+) and myeloid (CD11b+) cells in spleen is not significantly different between mice of both genotypes. Interestingly, within the myeloid compartment of the inguinal lymph node, we found a higher number of GFP cells. However, when normalized to total myeloid cell counts, the number of GFP+ cells was not significantly higher than GFP+ counts from control animals. Collectively, these results suggest *Gfral* is not expressed in immune cells from healthy mice.

Finally, we made use of publicly available single cell RNA-sequencing (scRNA-seq) labeled datasets to corroborate our results in human pediatric, adult and embryonic samples [22—28] (Figure 4). Except for rare cell expression in cortex, hippocampus and adult intestine tissue, we were unable to find *Gfral* expressing cells (Figure 4A) in pancreas, endometrium, pediatric and fetal intestine, and in immune cells in fetal tissue (Figure 4A; Supplemental Fig. 3). Additionally, the rare *GFRAL* expression was not associated with developmental stages or age (Supplemental Fig. 4).

Overall, our results show a conserved and restricted expression of GFRAL in the AP/NTS supporting a concentrated, rather than a diffuse, model of GDF15 action (Figure 4B).

4. DISCUSSION

In mammalian physiology individual peptide hormones are generally expressed by a small number of specialized cells within a single tissue and the respective receptor(s) are expressed broadly across many cell types and organs. Such is the case with insulin, glucagon, growth hormone and leptin [36—39]. However, the GDF15-GFRAL system seems to function uniquely as many different tissues and cell types can produce GDF15 but the expression of GFRAL, the only well-described receptor for GDF15, seems to be highly restricted to a single site across the entire body. GDF15 is the only known ligand for GFRAL and it regulates a range of physiologies including appetite, gastric motility, nausea and emesis, immune cell function and energy expenditure [4,9,12—15]. One possible mechanism to explain how GDF15 regulates such variate range of physiologic roles is that all these actions are solely mediated via GFRAL signaling on AP and NTS neurons, but a separate model proposes GDF15 acts on GFRAL expressing cells on peripheral tissues. To date, most reports support the former model with multiple analysis of *Gfral* mRNA using highly sensitive approaches failing to detect *Gfral* mRNA in brain regions outside the AP/NTS [12,16—18,20].

Within the periphery, experiments using transcriptomic approaches to measure mRNA such as qRT-PCR, have not found appreciable levels of *Gfral* in many peripheral tissues [9,12,16,18,20]. However, this does not rule out the existence of rare *Gfral*-expressing cell populations that mediate some of GDF15 effects in regions other than the AP/NTS. Indeed, a recent study observed GFRAL immunoreactivity in multiple peripheral tissues and even within central nervous system sites

beyond the AP/NTS [21], raising the possibility for the existence of uncharacterized GFRAL-expressing cells. As the GDF15/GFRAL axis is therapeutically tractable largely due to highly restricted GFRAL expression which limits off-target complications, the presence of GFRAL-expressing cell types outside the AP/NTS has direct implications on GDF15 and GFRAL-based therapies [40,41]. The antibody used in these studies has previously been shown to be specific for GFRAL within the AP/NTS [20], however, there is a lack of validation in other central nervous system sites and peripheral tissues where it may bind other proteins resulting in a false positive signal. Due to this, we sought to determine whether *Gfral* is expressed in peripheral tissues using three approaches.

First, smISH which is specific for targeted sequences, failed to detect *Gfral* mRNA in any mouse peripheral tissues we tested. Additionally, we used two genetic models to label *Gfral*-expressing cells with GFP either throughout development (*Gfral*^Cre^*::eGFP*) or specifically in the adult (*Gfral*^CreERT^*::eGFP*). Importantly, these genetic models have demonstrated a high concordance between Cre recombinase and *Gfral* using smFISH and translating ribosomal affinity purification (TRAP) [19]. Screening peripheral tissues for GFP-labelled cells, revealed rare GFP-labelled cells in kidney, pancreas and ovary. Of these tissues, GFP was also detected in the pancreas in the absence of Cre recombinase, suggesting a degree of "leak" in the Cre-dependent reporter depending on the tissue. Separately, we noted higher numbers of GFP+ myeloid cells of the lymph node, however this increase was not significantly higher than the number of GFP+ cells in control animals, likely due to autofluorescence. To complement the mouse experiments with human tissues, we examined a number of human immune-resident cells of the liver and the spleen from human tissue [25] but as the *GFRAL* gene was not mapped due to a complete lack of reads mapping to this gene. Therefore, within the datasets we could not acquire a plot or quantification of expression and further suggesting that *GFRAL* is not expressed by immune cells.

Additionally, we examined single cell sequencing data from eight human labeled datasets of non-brainstem cells including pancreas, endometrium, intestine, brain cortex, hippocampus and immune-resident cells of the liver, the spleen and tissues in development (e.g. yolk sac, liver, spleen, kidney, bone marrow) [22—28]. Similar to what we observed in the mouse, *GFRAL*-expressing cells in human tissues were undetectable in most analyzed tissues. In cortex, hippocampus and adult intestine we detected *GFRAL* + cells regardless of developmental stage, but critically these cells were extremely rare. This supports our proposed model of concentrated GDF15 action mediated via GFRAL expression in the AP/NTS. Indeed, specifically reducing *Gfral* expression within the brainstem abrogates GDF15's anorectic and energy expenditure promoting effects [42,43]. This further supports the concentrated GDF15 action model and thus reports describing functionally relevant GFRAL expression outside the brainstem require a high burden of evidence.

Limitations of our study include that we assume any *Gfral*^Cre^-expressing cell will also express GFP. However, this is not always the case as Cre-reporters do not fully represent their Cre-driver [44]. However, the lack of *Gfral* mRNA detected by *in-situ* hybridizations in these same tissues gives us confidence in our genetic approach to identify *Gfral*-expressing cells. Additionally, while we attempted to examine a broad range of tissue types, there are tissues and cell types not examined herein and these may warrant further investigation. Finally, as other TGFβ family receptor levels can be dramatically altered by infection and the immune cell activation [45], it is possible that in disease states, GFRAL is expressed on cell types it not under physiologic conditions.
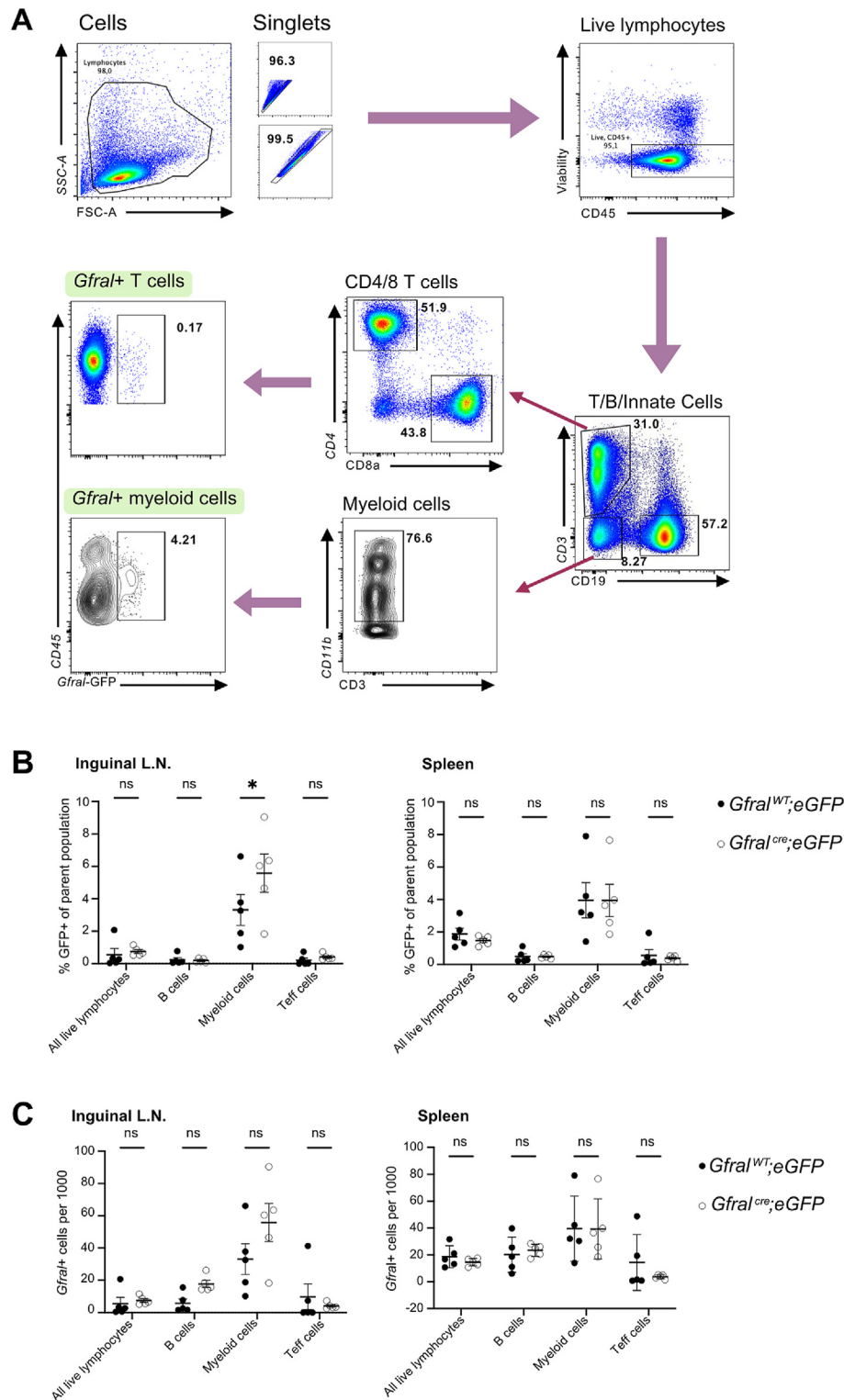
Figure 3: *Gfral* Cre reporter expression in immune cells. (A) Representative flow cytometry analysis of GFP reporter expression in CD45+ immune cells, further sub-gated by differential expression of CD4, CD8, CD11b, and CD19. (B) Mean frequency of GFP+ cells in the pre-gated parent population of cells taken from the inguinal lymph nodes (left) and spleen (right) ($n = 5$) compared to control ($n = 5$). (C) Mean count of GFP+ cells adjusted per 1000 cells in the pre-gated parent population of cells taken from the inguinal lymph nodes (left) and spleen (right) ($n = 5$) compared to controls ($n = 5$). Numbers in FACS plots indicate the frequencies of gated cells. Error bars, SEM. *p-value$\leq$0.05 determined by Two-Way ANOVA.

Abbreviations: eGFP = enhanced green fluorescent protein; GFP = enhanced green fluorescent protein; WT = wild-type; ns = non-significant; L.N. = lymph node; FACS=Fluorescence activated cell sorting; SEM = standard error of the mean.
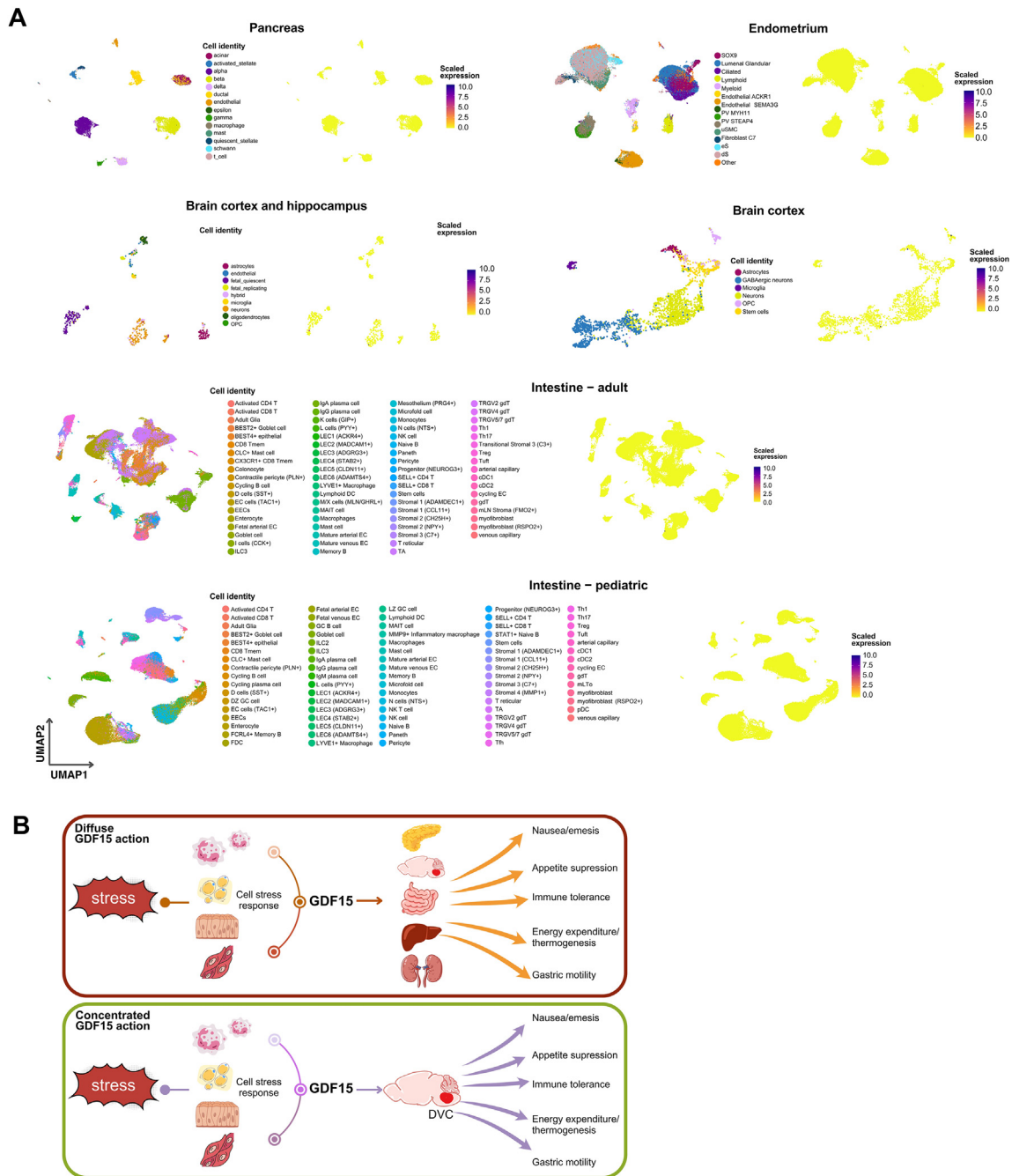
Figure 4: GFRAL expression in human tissues using scRNA-seq data. (A) UMAP plot of the scRNA-seq publicly available data on adult, pediatric and developmental tissues showing *Gfral* expression (right panels) on each cell type (left panels). (B) Models of the GDF15/GFRAL interaction proposed. The DVC includes the area postrema and the nucleus of the solitary tract.

Abbreviations: UMAP = uniform manifold approximation and projection; scRNA-seq = single-cell RNA-sequencing; OPC = oligodendrocyte precursor cell; GABA = gamma-aminobutyric acid; DVC = dorsal vagal complex; EECs = enteroendocrine cells; EC = enterochromaffin cells; ILC2 = type 2 innate lymphoid cells; ILC3 = type 3 innate lymphoid cells; LEC = lymphatic endothelial cells; DC = dentritic cells; MAIT = Mucosal Associated Invariant T; TA = transit amplifying; cDC1 = type-1 conventional dendritic cells; cDC2 = type-2 conventional dendritic cells; gdT = Gamma Delta T cells; mLN = mesenteric lymph node; Tmem = memory T cell; DZ = dark zone; LZ = light zone; GC = germinal centre; FDC = follicular dendritic cells; NK = natural killer; Tfh = T follicular helper; Th = T helper; Treg = regulatory T cells; mLTo = mesenchymal lymphoid tissue organizers; pDC = plasmacytoid dentritic cells; eS = endometrial stroma; dS = decidualized stroma; uSMC = uterine smooth muscle cells; PV = perivascular; GABA = Gamma-aminobutyric acid.

5. CONCLUSION

GDF15-GFRAL signaling is a critical mediator of the physiologic response to stress and activates numerous pathways that reduce appetite, alter gut motility, promote nausea, emesis and taste aversions while also increasing energy expenditure and regulating the immune system. As these pleiotropic effects could be mediated widespread GFRAL expression, we sought to quantify *Gfral*-labelled cells in multiple mouse and human tissues using highly sensitive and specific approaches. While *Gfral*-labelled cells could be detected in some tissues including mouse ovary and kidney, these cells were extraordinarily rare and importantly, not consistently detected using all methodologies. Together, our data supports the model wherein GDF15 action is overwhelmingly, if not exclusively, mediated by GFRAL expressed within the AP/NTS. As our understanding of GDF15 biology continues to expand beyond body weight control, the concentrated GDF15 action model should serve as a basis for our understanding of this intriguing hormone.

CRediT AUTHORSHIP CONTRIBUTION STATEMENT

Cecilia Hes: Writing — review & editing, Writing — original draft, Visualization, Software, Methodology, Investigation, Formal analysis, Data curation. **Luting Gui:** Writing — review & editing, Investigation. **Alexandre Bay:** Writing — review & editing, Writing — original draft, Visualization, Software, Investigation, Formal analysis, Data curation. **Fernando Alvarez:** Writing — review & editing, Visualization, Software, Investigation, Formal analysis, Data curation. **Pierce Katz:** Writing — review & editing, Investigation, Formal analysis. **Tanushree Paul:** Writing — review & editing, Investigation, Data curation. **Nadejda Bozadjieva-Kramer:** Writing — review & editing, Investigation, Funding acquisition. **Randy J. Seeley:** Writing — review & editing, Methodology, Conceptualization. **Ciriaco A. Piccirillo:** Writing — review & editing, Methodology, Conceptualization. **Paul Sabatini:** Writing — review & editing, Writing — original draft, Visualization, Methodology, Investigation, Funding acquisition, Formal analysis, Data curation, Conceptualization.

DECLARATION OF COMPETING INTEREST

RJS has received research support from Novo Nordisk, Fractyl, Astra Zeneca, Congruence Therapeutics, Eli Lilly, Bullfrog AI, Glycsend Therapeutics and Amgen. RJS has served as a paid consultant for Novo Nordisk, Eli Lilly, CinRx, Fractyl, Structure Therapeutics, Crinetics and Congruence Therapeutics. RJS has equity in Calibrate, Rewind and Levator Therapeutics. The remaining authors declare no competing interests.

APPENDIX A. SUPPLEMENTARY DATA

Supplementary data to this article can be found online at https://doi.org/10.1016/j.molmet.2024.102070.

DATA AVAILABILITY

Data will be made available on request.

REFERENCES

[1] Lockhart SM, Saudek V, O'Rahilly S. GDF15: a hormone conveying somatic distress to the brain. Endocr Rev 2020;41. https://doi.org/10.1210/endrev/bnaa007.

[2] Lawton LN, Bonaldo MF, Jelenc PC, Qiu L, Baumes SA, Marcelino RA, et al. Identification of a novel member of the TGF-beta superfamily highly expressed in human placenta. Gene 1997;203:17—26. https://doi.org/10.1016/S0378-1119(97)00485-X.

[3] Paralkar VM, Vail AL, Grasser WA, Brown TA, Xu H, Vukicevic S, et al. Cloning and characterization of a novel member of the transforming growth factor-beta/bone morphogenetic protein family. J Biol Chem 1998;273:13760—7. https://doi.org/10.1074/jbc.273.22.13760.

[4] Borner T, Shaulson ED, Ghidewon MY, Barnett AB, Horn CC, Doyle RP, et al. GDF15 induces anorexia through nausea and emesis. Cell Metabol 2020;31: 351—362 e5. https://doi.org/10.1016/j.cmet.2019.12.004.

[5] Breit SN, Johnen H, Cook AD, Tsai VW, Mohammad MG, Kuffner T, et al. The TGF-beta superfamily cytokine, MIC-1/GDF15: a pleotrophic cytokine with roles in inflammation, cancer and metabolism. Growth Factors 2011;29:187—95. https://doi.org/10.3109/08977194.2011.607137.

[6] Moore AG, Brown DA, Fairlie WD, Bauskin AR, Brown PK, Munier ML, et al. The transforming growth factor-beta superfamily cytokine MIC-1 is present in high concentrations in the serum of pregnant women. J Clin Endocrinol Metab 2000;85:4781—8. https://doi.org/10.1210/jcem.85.12.7007.

[7] Klein AB, Nicolaisen TS, Ortenblad N, Gejl KD, Jensen R, Fritzen AM, et al. Pharmacological but not physiological GDF15 suppresses feeding and the motivation to exercise. Nat Commun 2021;12:1041. https://doi.org/10.1038/s41467-021-21309-x.

[8] Lerner L, Tao J, Liu Q, Nicoletti R, Feng B, Krieger B, et al. MAP3K11/GDF15 axis is a critical driver of cancer cachexia. J Cachexia Sarcopenia Muscle 2016;7:467—82. https://doi.org/10.1002/jcsm.12077.

[9] Luan HH, Wang A, Hilliard BK, Carvalho F, Rosen CE, Ahasic AM, et al. GDF15 is an inflammation-induced central mediator of tissue tolerance. Cell 2019;178:1231—1244 e11. https://doi.org/10.1016/j.cell.2019.07.033.

[10] Brown DA, Moore J, Johnen H, Smeets TJ, Bauskin AR, Kuffner T, et al. Serum macrophage inhibitory cytokine 1 in rheumatoid arthritis: a potential marker of erosive joint destruction. Arthritis Rheum 2007;56:753—64. https://doi.org/10.1002/art.22410.

[11] Wollert KC, Kempf T, Peter T, Olofsson S, James S, Johnston N, et al. Prognostic value of growth-differentiation factor-15 in patients with non-ST-elevation acute coronary syndrome. Circulation 2007;115:962—71. https://doi.org/10.1161/CIRCULATIONAHA.106.650846.

[12] Yang L, Chang CC, Sun Z, Madsen D, Zhu H, Padkjaer SB, et al. GFRAL is the receptor for GDF15 and is required for the anti-obesity effects of the ligand. Nat Med 2017;23:1158—66. https://doi.org/10.1038/nm.4394.

[13] Borner T, Wald HS, Ghidewon MY, Zhang B, Wu Z, De Jonghe BC, et al. GDF15 induces an aversive visceral malaise state that drives anorexia and weight loss. Cell Rep 2020;31:107543. https://doi.org/10.1016/j.celrep.2020.107543.

[14] Chrysovergis K, Wang X, Kosak J, Lee SH, Kim JS, Foley JF, et al. NAG-1/GDF-15 prevents obesity by increasing thermogenesis, lipolysis and oxidative

metabolism. Int J Obes 2014;38:1555—64. https://doi.org/10.1038/ijo.2014.27.

[15] Wang D, Townsend LK, DesOrmeaux GJ, Frangos SM, Batchuluun B, Dumont L, et al. GDF15 promotes weight loss by enhancing energy expenditure in muscle. Nature 2023;619:143—50. https://doi.org/10.1038/s41586-023-06249-4.

[16] Li Z, Wang B, Wu X, Cheng SY, Paraoan L, Zhou J. Identification, expression and functional characterization of the GRAL gene. J Neurochem 2005;95:361—76. https://doi.org/10.1111/j.1471-4159.2005.03372.x.

[17] Emmerson PJ, Wang F, Du Y, Liu Q, Pickard RT, Gonciarz MD, et al. The metabolic effects of GDF15 are mediated by the orphan receptor GFRAL. Nat Med 2017;23:1215—9. https://doi.org/10.1038/nm.4393.

[18] Mullican SE, Lin-Schmidt X, Chin CN, Chavez JA, Furman JL, Armstrong AA, et al. GFRAL is the receptor for GDF15 and the ligand promotes weight loss in mice and nonhuman primates. Nat Med 2017;23:1150—7. https://doi.org/10.1038/nm.4392.

[19] Sabatini PV, Frikke-Schmidt H, Arthurs J, Gordian D, Patel A, Rupp AC, et al. GFRAL-expressing neurons suppress food intake via aversive pathways. Proc Natl Acad Sci U S A 2021;118. https://doi.org/10.1073/pnas.2021357118.

[20] Hsu JY, Crawley S, Chen M, Ayupova DA, Lindhout DA, Higbee J, et al. Non-homeostatic body weight regulation through a brainstem-restricted receptor for GDF15. Nature 2017;550:255—9. https://doi.org/10.1038/nature24042.

[21] Fichtner K, Kalwa H, Lin MM, Gong Y, Muglitz A, Kluge M, et al. GFRAL is widely distributed in the brain and peripheral tissues of mice. Nutrients 2024;16. https://doi.org/10.3390/nu16050734.

[22] Darmanis S, Sloan SA, Zhang Y, Enge M, Caneda C, Shuer LM, et al. A survey of human brain transcriptome diversity at the single cell level. Proc Natl Acad Sci U S A 2015;112:7285—90. https://doi.org/10.1073/pnas.1507125112.

[23] Baron M, Veres A, Wolock SL, Faust AL, Gaujoux R, Vetere A, et al. A single-cell transcriptomic map of the human and mouse pancreas reveals inter- and intra-cell population structure. Cell Syst 2016;3:346—360 e4. https://doi.org/10.1016/j.cels.2016.08.011.

[24] Zhong S, Zhang S, Fan X, Wu Q, Yan L, Dong J, et al. A single-cell RNA-seq survey of the developmental landscape of the human prefrontal cortex. Nature 2018;555:524—8. https://doi.org/10.1038/nature25980.

[25] Zhao J, Zhang S, Liu Y, He X, Qu M, Xu G, et al. Single-cell RNA sequencing reveals the heterogeneity of liver-resident immune cells in human. Cell Discov 2020;6:22. https://doi.org/10.1038/s41421-020-0157-z.

[26] Elmentaite R, Kumasaka N, Roberts K, Fleming A, Dann E, King HW, et al. Cells of the human intestinal tract mapped across space and time. Nature 2021;597:250—5. https://doi.org/10.1038/s41586-021-03852-1.

[27] Garcia-Alonso L, Handfield LF, Roberts K, Nikolakopoulou K, Fernando RC, Gardner L, et al. Mapping the temporal and spatial dynamics of the human endometrium in vivo and in vitro. Nat Genet 2021;53:1698—711. https://doi.org/10.1038/s41588-021-00972-2.

[28] Suo C, Dann E, Goh I, Jardine L, Kleshchevnikov V, Park JE, et al. Mapping the developing human immune system across organs. Science 2022;376:eabo0510. https://doi.org/10.1126/science.abo0510.

[29] Krashes MJ, Shah BP, Madara JC, Olson DP, Strochlic DE, Garfield AS, et al. An excitatory paraventricular nucleus to AgRP neuron circuit that drives hunger. Nature 2014;507:238—42. https://doi.org/10.1038/nature12956.

[30] Carpenter AE, Jones TR, Lamprecht MR, Clarke C, Kang IH, Friman O, et al. CellProfiler: image analysis software for identifying and quantifying cell phenotypes. Genome Biol 2006;7:R100. https://doi.org/10.1186/gb-2006-7-10-r100.

[31] Aran D, Looney AP, Liu L, Wu E, Fong V, Hsu A, et al. Reference-based analysis of lung single-cell sequencing reveals a transitional profibrotic macrophage. Nat Immunol 2019;20:163—72. https://doi.org/10.1038/s41590-018-0276-y.

[32] Korsunsky I, Millard N, Fan J, Slowikowski K, Zhang F, Wei K, et al. Fast, sensitive and accurate integration of single-cell data with Harmony. Nat Methods 2019;16:1289—96. https://doi.org/10.1038/s41592-019-0619-0.

[33] Li X, Eadara S, Jeon S, Liu Y, Muwanga G, Qu L, et al. Combined single-molecule fluorescence in situ hybridization and immunohistochemistry analysis in intact murine dorsal root ganglia and sciatic nerve. STAR Protoc 2021;2:100555. https://doi.org/10.1016/j.xpro.2021.100555.

[34] de Jager SC, Bermudez B, Bot I, Koenen RR, Bot M, Kavelaars A, et al. Growth differentiation factor 15 deficiency protects against atherosclerosis by attenuating CCR2-mediated macrophage chemotaxis. J Exp Med 2011;208:217—25. https://doi.org/10.1084/jem.20100370.

[35] Lodi RS, Yu B, Xia L, Liu F. Roles and Regulation of Growth differentiation factor-15 in the Immune and tumor microenvironment. Hum Immunol 2021;82:937—44. https://doi.org/10.1016/j.humimm.2021.06.007.

[36] Petersen MC, Shulman GI. Mechanisms of insulin action and insulin resistance. Physiol Rev 2018;98:2133—223. https://doi.org/10.1152/physrev.00063.2017.

[37] Habegger KM, Heppner KM, Geary N, Bartness TJ, DiMarchi R, Tschop MH. The metabolic actions of glucagon revisited. Nat Rev Endocrinol 2010;6:689—97. https://doi.org/10.1038/nrendo.2010.187.

[38] Dehkhoda F, Lee CMM, Medina J, Brooks AJ. The growth hormone receptor: mechanism of receptor activation, cell signaling, and physiological aspects. Front Endocrinol 2018;9:35. https://doi.org/10.3389/fendo.2018.00035.

[39] Myers Jr MG, Munzberg H, Leinninger GM, Leshan RL. The geometry of leptin action in the brain: more complicated than a simple ARC. Cell Metabol 2009;9:117—23. https://doi.org/10.1016/j.cmet.2008.12.001.

[40] Groarke JD, Crawford J, Collins SM, Lubaczewski S, Roeland EJ, Naito T, et al. Ponsegromab for the treatment of cancer cachexia. N Engl J Med 2024. https://doi.org/10.1056/NEJMoa2409515.

[41] Suriben R, Chen M, Higbee J, Oeffinger J, Ventura R, Li B, et al. Antibody-mediated inhibition of GDF15-GFRAL activity reverses cancer cachexia in mice. Nat Med 2020;26:1264—70. https://doi.org/10.1038/s41591-020-0945-x.

[42] Zhang SY, Bruce K, Danaei Z, Li RJW, Barros DR, Kuah R, et al. Metformin triggers a kidney GDF15-dependent area postrema axis to regulate food intake and body weight. Cell Metabol 2023;35:875—886 e5. https://doi.org/10.1016/j.cmet.2023.03.014.

[43] Tsai VW, Zhang HP, Manandhar R, Schofield P, Christ D, Lee-Ng KKM, et al. GDF15 mediates adiposity resistance through actions on GFRAL neurons in the hindbrain AP/NTS. Int J Obes 2019;43:2370—80. https://doi.org/10.1038/s41366-019-0365-5.

[44] Luo L, Ambrozkiewicz MC, Benseler F, Chen C, Dumontier E, Falkner S, et al. Optimizing nervous system-specific gene targeting with cre driver lines: prevalence of germline recombination and influencing factors. Neuron 2020;106:37—65 e5. https://doi.org/10.1016/j.neuron.2020.01.008.

[45] McCartney-Francis NL, Wahl SM. Transforming growth factor beta: a matter of life and death. J Leukoc Biol 1994;55:401—9. https://doi.org/10.1002/jlb.55.3.401.